energies

MDPI

Article

Application of a Magnetic Field in Saturated Film Boiling of a Magnetic Nanofluid (MNF) under Reduced Gravity

Kaikai Guo [1,2,3], Fucheng Chang [1] and Huixiong Li [1,*]

[1] State Key Laboratory of Multiphase Flow in Power Engineering, Xi'an Jiaotong University, Xi'an 710049, China; kaixinguo1022@126.com (K.G.); changfucheng1996@stu.xjtu.edu.cn (F.C.)
[2] Facility Design & Instrumentation Institute, China Aerodynamics Research and Development Center, Mianyang 621000, China
[3] State Key Laboratory of Aerodynamics, China Aerodynamics Research and Development Center, Mianyang 621000, China
* Correspondence: huixiong@mail.xjtu.edu.cn; Tel.: +86-29-82668767

Abstract: To overcome the problem of abnormally large bubbles and the large reduction of heat flux under low gravity, the computational model of magnetic nanofluid (MNF) boiling flow was used to systematically study the thermodynamic characteristics of an MNF-saturated film boiling with and without the magnetic field. This study found that in the absence of a magnetic field, the decrease of the gravity level makes the bubble size increase and the bubble departure time increase, and the lower the gravity level, the worse the boiling heat transfer. However, after applying the magnetic field, bubble size decreases significantly and the bubble departure time is shortened. As the magnetic field intensity increases, the difference in bubble size and heat transfer characteristics between different gravity levels becomes smaller and smaller, which shows that for the boiling flow of MNF under low gravity levels, applying a magnetic field can effectively avoid the appearance of abnormally large bubbles, enhance heat transfer, and improve the safety of related heat transfer equipment.

Keywords: magnetic nanofluid (MNF); reduced gravity; film boiling; enhanced heat transfer

Citation: Guo, K.; Chang, F.; Li, H. Application of a Magnetic Field in Saturated Film Boiling of a Magnetic Nanofluid (MNF) under Reduced Gravity. *Energies* **2021**, *14*, 634. https://doi.org/10.3390/en14030634

Received: 17 December 2020
Accepted: 7 January 2021
Published: 27 January 2021

1. Introduction

Boiling and condensation are considered to be the most effective means of heat transfer in many types of technical equipment. Because of the large density differences between gases and liquids, buoyancy is of vital importance in controlling the physical process of two-phase flow, and most of the relations of boiling heat transfer include the influence of gravity and buoyancy force. A change in gravity will strongly affect the momentum and energy transfer, and it causes the phase separation phenomenon to be more difficult. Therefore, under different gravity conditions, especially under low gravity levels, research on boiling performance will show different characteristics.

In comparison with conventional gravity conditions on Earth, the problem of boiling heat transfer under reduced gravity is more complicated. The abnormally large bubbles and the significant reduction of heat flux under reduced gravity may cause unsafe operation of heat dissipation equipment, and may even deteriorate heat transfer, resulting in damage to the equipment, which makes it difficult for boiling to achieve its advantages in future space systems. Therefore, how to reduce or even eliminate the effect of gravity on two-phase boiling, how to suppress the occurrence of abnormally large bubbles, and how to prevent the heat flux from drastically reducing will be the key to enhancing boiling heat transfer under reduced gravity.

Experimental and numerical methods have been used to study boiling heat transfer under reduced gravity levels. Experiments have been conducted on reduced gravity through the Drop Tower [1], Drop Shaft [2], Parabolic Flight [3], Sounding Rocket [4], and NASA's Space Shuttle [5] and Space Station (International Space Station (ISS)) [6]. Boiling

experiments under reduced gravity are characterized by high costs, complex hardware, short durations, and great difficulties in control, making the existing data on boiling heat transfer under reduced gravity scarce [7]. Because of the difficulty of implementing reduced-gravity boiling experimental studies, researchers are limited in studying the reduced-gravity boiling phenomenon with experimental method. With the development of computational methods and computer performance, numerical study has become a very effective method for reduced-gravity boiling research. Numerical simulations are easier to implement and make it easier to obtain more details than experimental methods, and thus help to better understand the heat transfer mechanism under reduced gravity. In the last few decades, great efforts have been made to improve the numerical simulation methods for two-phase flow and phase change, and many scholars [8–10] have used these methods to study boiling performance under reduced gravity.

As we all know, various working fluids have various heat transfer performances. The choice of an appropriate heat transfer working fluid has a crucial effect on boiling heat transfer characteristics under reduced gravity. As a recent type of heat transfer working fluid, a magnetic nanofluid (MNF) can effectively improve heat transfer performance. Many scholars [11–15] have conducted experiments to study MNFs' boiling heat transfer performance, and have made important progress. However, most of the research on the boiling heat transfer of MNFs is carried out on Earth, and the relevant research under reduced gravity is rarely published. In our previous study [16,17], a numerical simulation for MNF film boiling was developed to investigate the heat transfer performance and dynamic characteristics by applying a uniform and non-uniform magnetic field. The results showed that the magnetic field could greatly strengthen an MNF's boiling heat transfer. In view of this, we believe that an external magnetic field can effectively weaken or even eliminate the effect of reduced gravity and further enhance the boiling heat transfer under reduced gravity. In this paper, the heat transfer characteristics and thermodynamic characteristics of the phase interface of an MNF-saturated film boiling under different levels of reduced gravity will be further studied in detail by exploring the multiple physical-field couplings between different gravity fields and the velocity field, pressure field, temperature field, phase field, and magnetic field, further revealing the enhancement mechanism of the MNF's boiling heat transfer by applying the magnetic field under the influence of different gravitational fields.

2. Numerical Modeling

Aiming at a problem that is rarely reported in the study of the phase-interface evolution of MNF boiling heat transfer, the basic computational model of two-phase boiling flow should be solved, and then the coupled magnetic field computational model and magnetic field force model should be developed on the basis of this basic computational model. The details will be described below.

2.1. Interface Tracking

The dynamic characteristics of bubbles have a very important influence on the boiling heat transfer. Great efforts have been made to improve the numerical simulation performance for two-phase flow [18–20]. In this study, the coupled volume-of-fluid (VOF) and level-set (LS) (VOSET) method [21] was adopted to achieve the capture of the phase interface. Please refer to Refs. [21,22] to obtain the specific implementation methods for the VOSET method.

On the basis of the LS function ϕ calculated by the VOSET method, the interface curvature is calculated, and the physical properties near the phase interface are smoothed. Then, the surface tension applied to the phase interface is calculated. In a two-dimensional rectangular coordinate system, the curvature $\kappa(\phi)$ is calculated as follows:

$$\kappa(\phi) = \nabla \cdot \left(\frac{\nabla \phi}{|\nabla \phi|} \right) = \frac{\phi_{xx}\phi_y^2 - 2\phi_{xy}\phi_x\phi_y + \phi_{yy}\phi_x^2}{\left(\phi_x^2 + \phi_y^2\right)^{3/2}} \quad (1)$$

The density, viscosity, thermal conductivity, specific heat, and magnetic permeability can be calculated as:

$$\rho(\phi) = \rho_g H(\phi) + \rho_l(1 - H(\phi)) \tag{2}$$

$$\eta(\phi) = \eta_g H(\phi) + \eta_l(1 - H(\phi)) \tag{3}$$

$$\lambda(\phi) = \lambda_g H(\phi) + \lambda_l(1 - H(\phi)) \tag{4}$$

$$c_p(\phi) = c_{p,g} H(\phi) + c_{p,l}(1 - H(\phi)) \tag{5}$$

$$\mu(\phi) = \mu_g H(\phi) + \mu_l(1 - H(\phi)) \tag{6}$$

where the subscripts g and l represent the continuous phase and the discrete phase, respectively. $H(\phi)$ is the smooth Heaviside function, which can better smooth the physical properties, and its expression is:

$$H(\phi) = \begin{cases} 0 & \text{when } \phi < -s \\ \frac{1}{2}\left[1 + \frac{\phi}{s} + \frac{1}{\pi}\sin\left(\frac{\pi\phi}{s}\right)\right] & \text{when } |\phi| < s \\ 1 & \text{when } \phi > s \end{cases} \tag{7}$$

where s is the width of the transition region for smoothing and is equal to 1.5 h, and h represents the grid size.

According to the continuous surface force (CSF) model [23], the surface tension $\mathbf{F}_\sigma$ can be computed in the form of the level-set function:

$$\mathbf{F}_\sigma = -\sigma\kappa(\phi)\delta(\phi)\nabla\phi \tag{8}$$

where σ and $\delta(\phi)$ represent the surface tension coefficient and Dirac delta function, respectively. $\delta(\phi)$ can be expressed as

$$\delta(\phi) = \frac{\partial H(\phi)}{\partial \phi} = \begin{cases} 0 & \text{when } |\phi| > s \\ \frac{1}{2s}\left[1 + \cos\left(\frac{\pi\phi}{s}\right)\right] & \text{when } |\phi| \le s \end{cases} \tag{9}$$

2.2. Governing Equations

As the boiling problem of MNF is relatively complex, the following assumptions will be made to solve the MNF boiling problem:

- We assume that magnetic nanoparticles are uniformly dispersed in the base fluid and there is no interaction between the particles, that is, no agglomeration and deposition phenomena occur. Therefore, the MNF can be considered as a homogeneous fluid with the same properties;
- The volume concentration of the MNF does not change during the boiling process;
- We do not consider the changes of the magnetic field in the MNF's physical properties and volume concentration;
- The MNF is non-conductive.

Regarding the boiling problem of the viscous incompressible two-phase flow of the MNF under the action of the magnetic field, the conservation equations contain the momentum equation, which includes the magnetic force, the Maxwell equation of static magnetic field, etc. The involved models also include the magnetic field force model.

Assuming that the MNF is non-conductive and no displacement current appears, Maxwell's equations could be expressed as:

$$\nabla \times \mathbf{H} = 0 \tag{10}$$

$$\nabla \cdot \mathbf{B} = 0 \tag{11}$$

where $\mathbf{B}$ represents the magnetic induction intensity and $\mathbf{H}$ represents the magnetic field intensity. According to magnetization equilibrium theory, the magnetization $\mathbf{M} = \chi\mathbf{H}$; χ is the magnetic susceptibility, $\chi = \mu/\mu_0 - 1$, μ is the relative permeability, and μ_0 is the vacuum permeability; the relationship among $\mathbf{B}$, $\mathbf{H}$, and $\mathbf{M}$ could be expressed as:

$$\mathbf{B} = \mu_0(1+\chi)\mathbf{H} = \mu\mathbf{H} \tag{12}$$

$$\mathbf{B} = \mu_0(1+\chi)\mathbf{H} = \mu_0(\mathbf{H}+\mathbf{M}) \tag{13}$$

We introduce the scalar magnetic potential ψ, define $\mathbf{H} = -\nabla\psi$, and further simplify the Maxwell Equations (10) and (11) into the Laplace form about the magnetic potential ψ:

$$\nabla \cdot (\mu \nabla \psi) = 0 \tag{14}$$

At the phase interface of the MNF, the magnetic field satisfies certain boundary conditions: The normal direction of the **B** field is continuous, and the tangential direction of the **H** field is continuous, that is, $\mathbf{B}_1$, $\mathbf{H}_1$, $\mathbf{B}_2$, and $\mathbf{H}_2$ on both sides of the interface meet the following conditions:

$$\mathbf{n} \cdot (\mathbf{B}_1 - \mathbf{B}_2) = 0 \tag{15}$$

$$\mathbf{n} \times (\mathbf{H}_1 - \mathbf{H}_2) = 0 \tag{16}$$

For incompressible two-phase boiling problems with phase changes, the conservation equations can be expressed as:

$$\nabla \cdot \mathbf{u} = \dot{m}\left(\frac{1}{\rho_g} - \frac{1}{\rho_l}\right) \tag{17}$$

$$\rho\left(\frac{\partial \mathbf{u}}{\partial \mathrm{t}} + \mathbf{u} \cdot \nabla \mathbf{u}\right) = -\nabla p + \nabla \cdot \left[\eta\left((\nabla \mathbf{u}) + (\nabla \mathbf{u})^{\mathrm{T}}\right)\right] + \rho \mathbf{g}(1 - \beta_T(T - T_{sat})) + \mathbf{F}_\sigma + \mathbf{F}_m \tag{18}$$

$$\frac{\partial T}{\partial t} + \mathbf{u} \cdot \nabla T = \frac{\lambda}{\rho c_p}\nabla^2 T \tag{19}$$

$$\frac{\partial c}{\partial t} + \mathbf{u} \cdot \nabla c = \frac{\dot{m}}{\rho_g} \tag{20}$$

where $\dot{m}$ is the mass transfer rate. $\mathbf{F}_m$ represents the magnetic force.

In a cell with a phase interface, assuming that Ω represents the control volume unit and Γ is the phase interface in Figure 1, the following relationship is satisfied:

$$\int_{\Omega} \dot{m} dV = \frac{1}{h_{lg}} \int_{\Gamma} \dot{q} dA \tag{21}$$

where h_{lg} represents the latent heat of vaporization; $\dot{q}$ is the heat flux that causes the phase change at the phase interface, and its expression is

$$\dot{q} = \lambda_g \left.\frac{\partial T}{\partial n}\right|_g - \lambda_l \left.\frac{\partial T}{\partial n}\right|_l \tag{22}$$

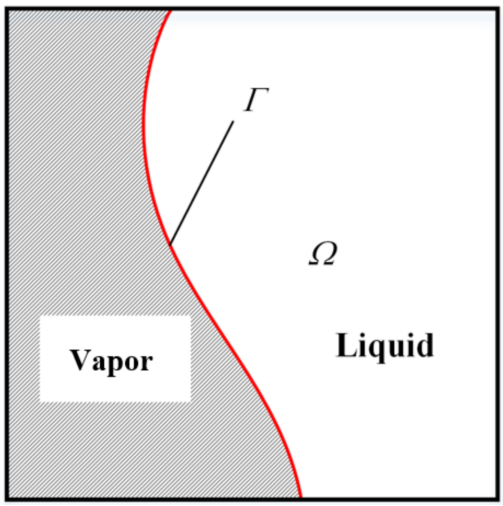

Figure 1. Schematic of a cell with a phase interface.

Equation (22) establishes the relationship between the temperature field and the mass transfer rate $\dot{m}$ of the phase change, which is also called the Stefan condition on the phase interface. In this way, the solution of the mass transfer rate $\dot{m}$ is transformed into the solution of the temperature gradient on both sides of the phase interface. Because the phase interface temperature is assumed to be the saturation temperature, the temperature field near the phase interface and the cell center temperature are needed to obtain the temperature gradient.

In this paper, the processing method of Ling et al. [24] was adopted to calculate the cell temperature with the phase interface. Figure 2 is an example to introduce this computing method for a cell with a phase interface, and the linear interpolation method is used to calculate the temperature. If the cell center is in the vapor phase, we look for the interpolation point A' along the normal direction of the phase interface. The distance from point A' to the center point A of the cell with a phase interface is d. Then, the temperature T_A of the point A is estimated according to the distance $|\phi_A|$ between the center point A and phase interface. If the cell center with the phase interface is located in the liquid phase, the temperature T_B of the cell center B is calculated in the above way. The temperature of the phase interface grids could be expressed by the formula:

$$\frac{T_A - T_{sat}}{T_{A'} - T_{sat}} = \frac{|\phi_A|}{|\phi_A| + d} \tag{23}$$

$$\frac{T_B - T_{sat}}{T_{B'} - T_{sat}} = \frac{|\phi_B|}{|\phi_B| + d} \tag{24}$$

where the temperatures $T_{A'}$ and $T_{B'}$ of the interpolation points A' and B' can be obtained by interpolating the temperatures of the surrounding grids around the interpolation points.

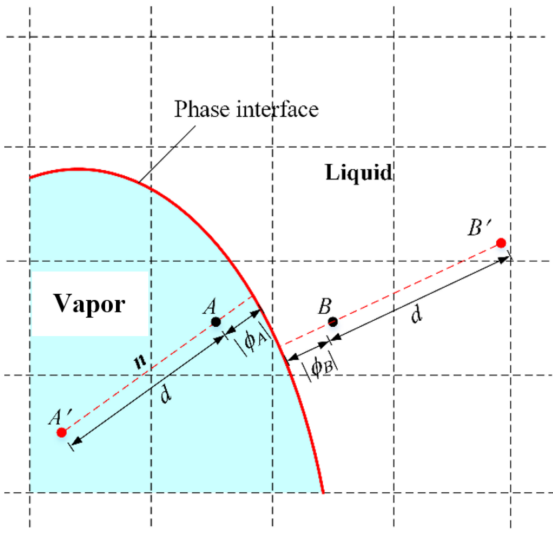

Figure 2. Schematic of the solution method for the temperature at the center point of the cell containing the phase interface.

As for the temperature gradient on both sides of the phase interface, the normal probe technique proposed by Udaykumar [25] and the bilinear interpolation method [24] were used for the calculations in this paper. Figure 3 displays a schematic of the calculating method. When this phase interface is reconstructed with the Piecewise Linear Interface Calculation (PLIC) method, the linear segment is used to reconstruct the phase interface. For the phase interface grids, the center point coordinate (point A in Figure 3) can be obtained by taking the average value of the coordinates of the two vertices of the corresponding straight line segment. The temperature gradients in the liquid phase and vapor phase at the phase interface in this grid cell are expressed by the temperature gradient at point A in the normal direction. At each phase, along the positive and negative normal direction,

there are two points (A_1 and A_2 or A_3 and A_4), whose distances from the center point A are d and $2d$, respectively, as shown in Figure 3. Finally, the quadratic approximation method was used to estimate the normal temperature gradient of the phase interface, expressed as:

$$\left.\frac{\partial T}{\partial n}\right|_g \approx \frac{-T_{A_2} + 4T_{A_1} - 3T_{sat}}{2d} \tag{25}$$

$$\left.\frac{\partial T}{\partial n}\right|_l \approx \frac{-T_{A_4} + 4T_{A_3} - 3T_{sat}}{2d} \tag{26}$$

where the temperatures of A_1 and A_2 as well as A_3 and A_4 can be obtained by interpolating the temperatures of the surrounding grids around them. Finally, the temperature gradient on both sides can be obtained, so that phase change rate $\dot{m}$ is calculated through Equations (21) and (22). The final expression of the phase change rate $\dot{m}$ is:

$$\int_\Omega \dot{m} dV = \frac{1}{h_{lg}} \left(\lambda_g \left.\frac{\partial T}{\partial n}\right|_g - \lambda_l \left.\frac{\partial T}{\partial n}\right|_l \right) \Delta A \tag{27}$$

where ΔA is the area of the phase interface and can be obtained through the geometric method.

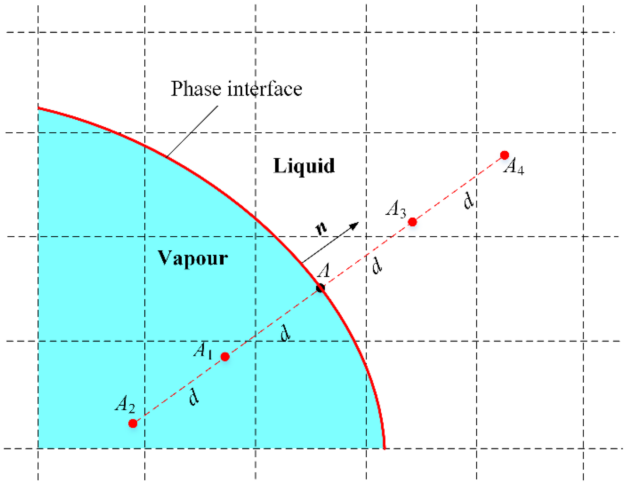

Figure 3. Schematic of the normal probe technique.

The magnetic force $\mathbf{F}_m$ could be calculated by Rosensweig [26], who expressed it as:

$$\mathbf{F}_m = -\frac{1}{2} H^2 \nabla \mu \tag{28}$$

By substituting Equation (6) into Equation (14), $\mathbf{F}_m$ can be further transformed:

$$\mathbf{F}_m = -\frac{1}{2} H^2 (\mu_1 - \mu_g) \delta(\phi) \nabla \phi \tag{29}$$

According to the previous assumptions, the MNF can be approximated as a single-phase fluid [26]. The density, specific heat, thermal conductivity, and viscosity can be calculated as follows [26]:

$$\rho_{mix} = (1 - \varphi)\rho_l + \varphi \rho_p \tag{30}$$

$$c_{p,mix} = \frac{(1 - \varphi)\rho_l c_{p,l} + \varphi \rho_p c_{p,p}}{\rho_{mix}} \tag{31}$$

$$\lambda_{mix} = \left(\frac{\lambda_p + 2\lambda_l - 2\varphi(\lambda_l - \lambda_p)}{\lambda_p + 2\lambda_l + \varphi(\lambda_l - \lambda_p)} \right) \lambda_l \tag{32}$$

$$\eta_{mix} = (1 + 2.5\varphi)\eta_l \tag{33}$$

where φ is the volume concentration of the MNF. The subscript p stands for magnetic nanoparticles.

The above description is the process of establishing the boiling flow and heat transfer model of an incompressible two-phase MNF in a magnetic field. The accuracy of the computational model's application in uniform and non-uniform magnetic fields was verified in References [16,17], and repeated verification will not be performed here. The physical properties of the MNF adopted in this paper are displayed in Table 1.

Table 1. Properties of the magnetic nanofluid (MNF).

	Liquid	Vapor	Nanoparticle
Density (kg/m^3)	200.0	5.0	5600.0
Thermal conductivity (W/m·K)	40.0	1.0	6.0
Thermal capacity (J/kg·K)	400.0	200	670.0
Dynamic viscosity (kg/m·s)	0.1	0.005	
Surface tension coefficient (N/m)	0.1		
Latent heat (J/kg)	10,000.0		
Magnetic susceptibility	0.2		

3. Results and Discussion

3.1. Effect of the Uniform Magnetic Field

3.1.1. Effect of the Magnetic Field under Terrestrial Gravity

Firstly, the effect of magnetic field intensity on the MNF's boiling curve under terrestrial gravity is introduced. The wall superheat is selected in the range between 1 and 10 K. Figure 4 displays the influence of the magnetic field on the boiling curve under terrestrial gravity. In Figure 4, after applying the magnetic field, the boiling heat transfer characteristics of the MNF can be enhanced. Therefore, the magnetic field has a crucial influence on the MNF's boiling heat transfer characteristics under terrestrial gravity. It is speculated that the application of the magnetic field may solve the problems of large bubbles escaping and the heat flux decreasing in the boiling process under reduced gravity or even microgravity. The details will be described below.

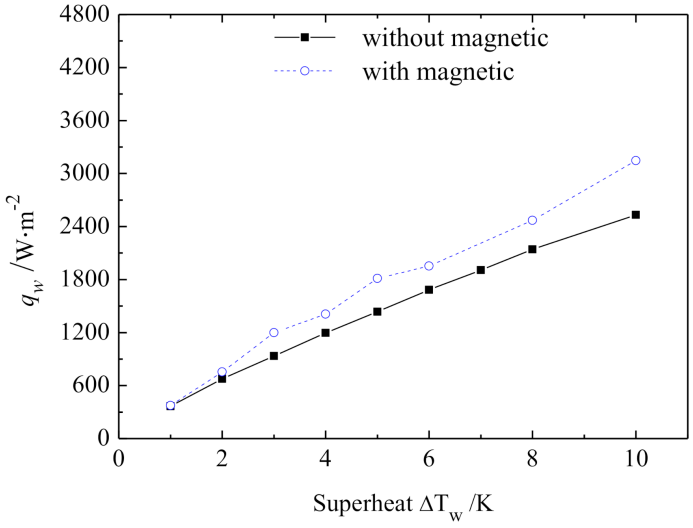

Figure 4. Influence of the magnetic field intensity on the boiling curve under terrestrial gravity.

3.1.2. Phase Interface Evolution

Figure 5 shows the influence of the magnetic field on the bubble departure under reduced gravity. Here, the superheat was 2 K and the relative gravity levels (g/g_e) were 1.0, 0.44, and 0.11, respectively. The magnetic field intensities applied were 5, 10, 15, 20, and 30 kA/m, respectively. A comparison of phase interface evolution with and without a magnetic field was studied.

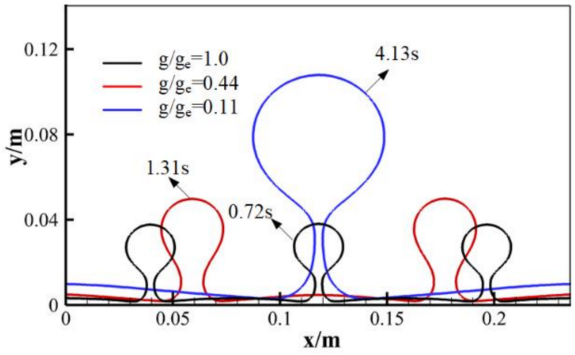

(**a**)

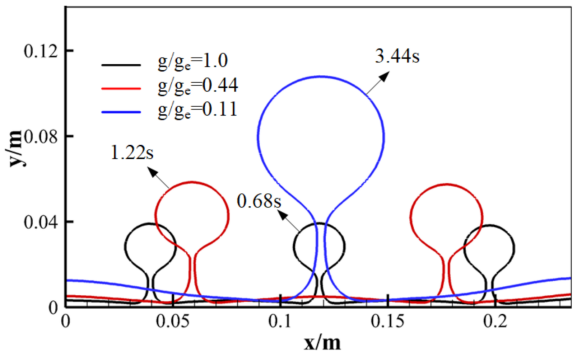

(**b**)

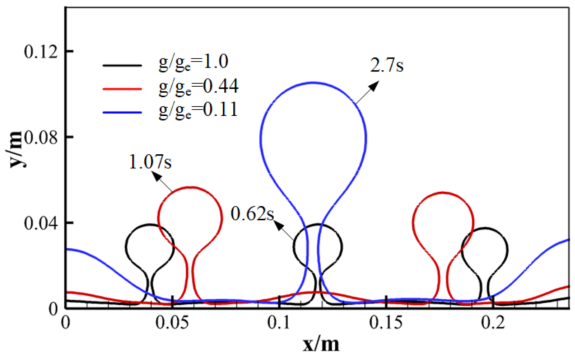

(**c**)

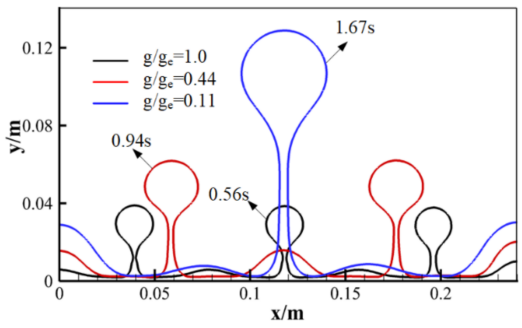

(**d**)

Figure 5. *Cont*.

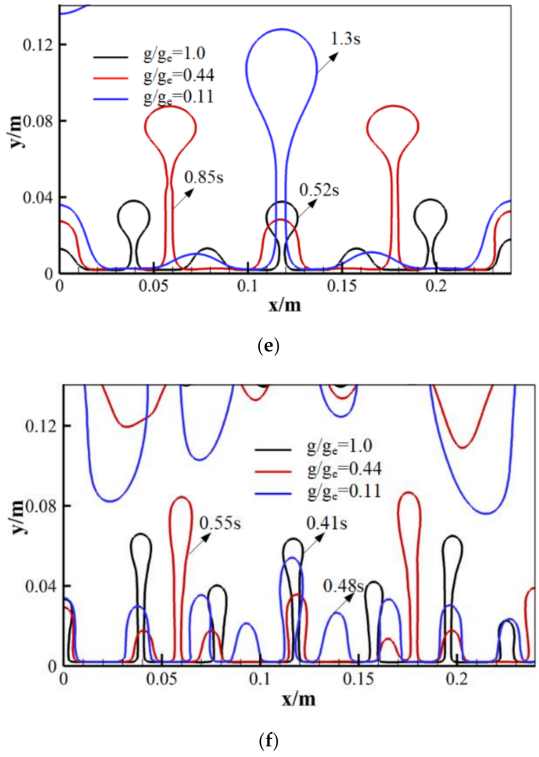

Figure 5. Phase interface evolution when applying a magnetic field. (**a**) H_0 = 0 kA/m, (**b**) H_0 = 5 kA/m, (**c**) H_0 = 10 kA/m, (**d**) H_0 = 15 kA/m, (**e**) H_0 = 20 kA/m, and (**f**) H_0 = 30 kA/m.

In the film boiling, the heat flux through the vapor region from the superheated wall causes the vaporization of the adjacent liquid near the phase interface. Because of the density difference of the vapor phase and the liquid phase, the continuously generated vapor grows and forms bubbles under the action of buoyancy, and then the bubbles detach and rise. With the decrease of gravity, the buoyancy decreases and the bubble motion is restrained. The departure of boiling bubbles without a magnetic field is displayed in Figure 5a, from which we can see that the bubble size increases as the gravity decreases. As the gravity decreases, the separation distance between neighboring bubble generation sites increases dramatically. At any given gravity level, the number of bubbles in the fixed calculation domain needs to stay consistent with the wavelength calculated with the Taylor–Helmholtz instability. When g/g_e = 1.0, the number of bubbles is 3, which is consistent with the Taylor–Helmholtz instability; when g/g_e = 0.44, the number is reduced to 2; when g/g_e = 0.11, the reduction of this number to 1 is also consistent with the instability requirement of this gravity condition. Figure 5a also shows the bubble detachment times under different gravity levels the bubble detachment time of the first set increases as the gravity decreases.

The influence of the magnetic field intensity on phase interface evolution in the MNF film boiling under terrestrial gravity is described in detail in our previous study [16]. The conclusion is that the increase of magnetic field intensity causes the number of bubble formation sites to increase; the bubble morphology with a magnetic field changes significantly, which can also be clearly seen in Figure 5. The effect of the magnetic field on the evolution of the phase interface at different gravity levels is displayed in Figure 5b–f. From Figure 5b–f, we can see that by applying the magnetic field, the influence of the magnetic field on the phase interface evolution mode at other low gravity levels is basically the same as that under terrestrial gravity. As mentioned above, under reduced gravity, the effect of buoyancy is weakened; it is easy to form large bubbles, and it is not easy to release them, which is obviously not conducive to the heat dissipation of the heating surface. When applying the magnetic field, with the increase of magnetic field intensity, the bubble size decreases, the bubble detachment time decreases, and detachment of the bubbles become

more intense. Moreover, as the magnetic field intensity increases, the differences among the phase interface evolutions under different gravity levels become smaller and smaller. When the intensity increases to 30 kA/m, the flow state changes from the bubble flow without the magnetic field to vapor column flow, and then the evolution modes of the phase interface under different gravity levels are basically the same. The reason is that the magnetic field indirectly compensates for the loss of gravity under reduced gravity. If the magnetic field intensity increases to a sufficiently large value, the magnetic force will be greater than the buoyancy. Therefore, at a low gravity level, the magnetic field of a certain intensity can be applied to restore and control the length scale and time scale under terrestrial gravity. The above results indicate that an applied magnetic field can effectively solve the problem of large bubbles being generated during the boiling process under reduced gravity, and can also make the boiling process under reduced gravity tend to be consistent with the boiling process under terrestrial gravity.

3.1.3. Heat Transfer Characteristics

Figure 6 gives the influence of magnetic field intensity on the space-averaged heat flux over time at various gravity levels, and Figure 7 also plots the influence of the magnetic field on the averaged heat flux and heat flux enhancement ratio e at different gravity levels. The parameter e represents the heat flux enhancement ratio, which is the ratio between the heat flux at another magnetic field intensity and the heat flux without a magnetic field at any fixed gravity level. Without a magnetic field, the space- and time-averaged heat flux at the three gravity levels of g/g_e = 1.0, 0.44, and 0.11 are 677, 513, and 258 W/m^2, respectively, as shown in Figures 6a and 7a.

From the above results, we can see that heat flux decreases as the gravity level decreases. This also reflects the second problem of the boiling phenomenon under reduced gravity that was mentioned above, that is, the problem of heat flux reduction. Improving this problem is very important for boiling heat transfer enhancement under reduced gravity. As shown in Figure 6a–d, the reduction of the gravity level can delay the bubble detachment from the vapor film, and the heat transfer rate of the heating surface becomes worse. After applying the magnetic field, the bubble detachment frequency increases and the heat transfer coefficient is improved. The variations of the space- and time- averaged heat flux under certain magnetic field intensities at three gravity conditions are listed in Table 2. From Figures 6 and 7 and Table 2, it can be seen that, as the magnetic field intensity increases, the difference between the space-averaged heat flux over time at the three gravity levels becomes smaller and smaller, and the difference between the averaged heat flux also becomes smaller and smaller. The heat flux enhancement ratio e at all three gravity levels increases when the magnetic field intensity increases. However, with the decrease of the gravity level, the slope of the variation curve of the heat flux enhancement ratio e becomes larger and larger, indicating that the lower the gravity level, the greater the effect of the magnetic field on boiling heat transfer.

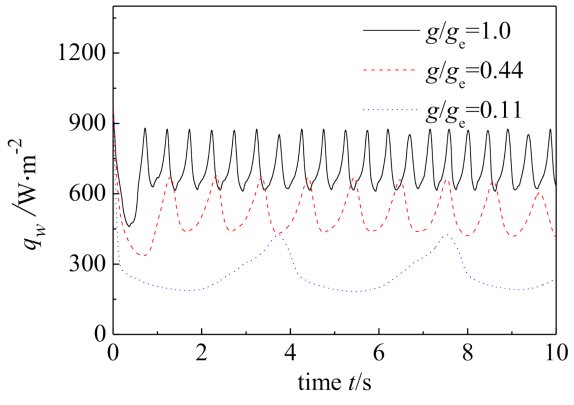

(a)

Figure 6. *Cont.*

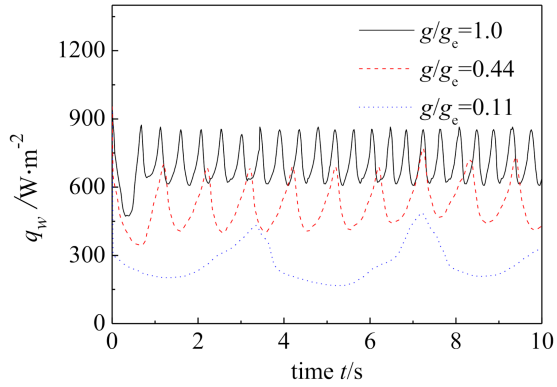

(**b**)

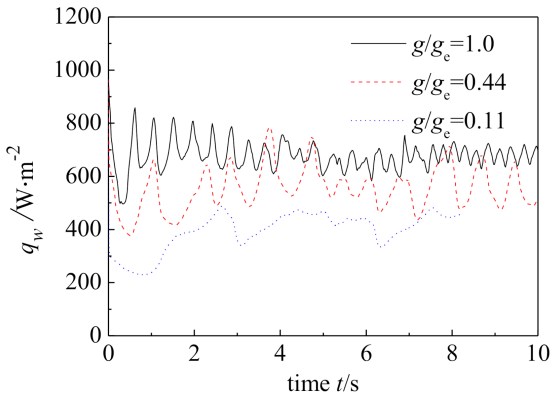

(**c**)

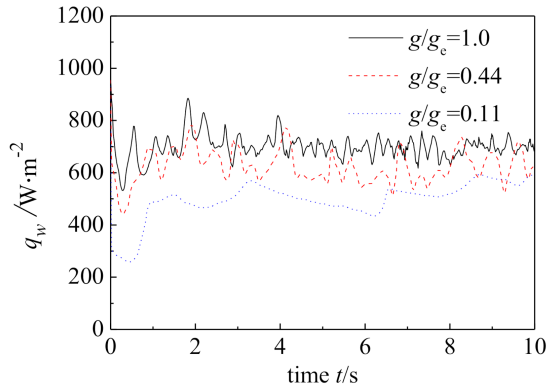

(**d**)

Figure 6. Effect of magnetic field intensity on the variation of the space-averaged heat flux with time. (**a**) H_0 = 0 kA/m, (**b**) H_0 = 5 kA/m, (**c**) H_0 = 10 kA/m, and (**d**) H_0 = 15 kA/m.

Table 2. Averaged heat flux and heat flux enhancement ratio under a uniform magnetic field.

g/g_e	q_0/(W/m^2)	5 kA/m		10 kA/m		15 kA/m		20 kA/m	
		q_m/(W/m^2)	e	q_m/(W/m^2)	e	q_m/(W/m^2)	e	q_m/(W/m^2)	e
1.0	677	677	1.00	678	1.00	700	1.03	755	1.11
0.44	513	518	1.01	554	1.08	627	1.22	665	1.30
0.11	258	267	1.03	394	1.53	497	1.93	572	2.22

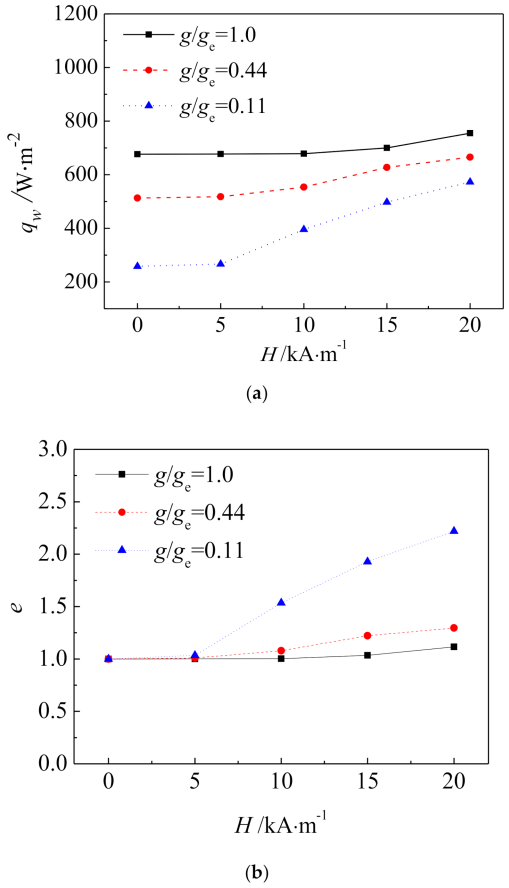

Figure 7. The variations of the (**a**) averaged heat flux and (**b**) heat flux enhancement ratio with magnetic field intensity H at different gravity levels under a uniform magnetic field.

3.2. Effect of a Non-Uniform Magnetic Field

In our previous studies [16,17], the effects of uniform and non-uniform magnetic fields on MNF heat transfer and the phase interface thermodynamics of a film boiling under terrestrial gravity were introduced in detail. The results of the two magnetic fields are clearly different. In Section 3.1, the influence of a uniform magnetic field on the MNF film boiling under reduced gravity was introduced. Therefore, it is necessary to study the influence of a non-uniform magnetic field on the MNF film boiling under reduced gravity in order to reveal the different effects and mechanisms of the magnetic field on the film boiling at reduced gravity by applying a uniform and non-uniform magnetic field. The computational setup adopted in this section is exactly the same as that in our previous study [17], and the wall superheat is uniformly set at 2 K.

3.2.1. Phase Interface Evolution

Figure 8 displays the influence of non-uniform magnetic fields on the first set of bubble departures at different gravity levels. Figure 8 also plots the variation curve of the first set of bubble departure times under different magnetic field intensities. The influence of the non-uniform magnetic field on bubble detachment is both identical and different at the three different gravity levels. The identical part is that, as the intensity increases, both the bubble departure time and the bubble departure diameter gradually decrease. The difference is that although the variation trend is the same, the influence degree is different, that is, with the decrease of the gravity level, the influence of the magnetic field on bubble detachment becomes more and more obvious. In addition, from Figures 8 and 9, it can be concluded that the increase of the magnetic field intensity makes the differences in the bubble detachment at the three gravity levels become smaller and smaller, especially when

the gravity level drops to g/g_e = 0.11; then, the bubble departure time is almost equal. From this point of view, this also shows that when the magnetic field is applied, it is possible to control the boiling phenomenon at a reduced gravity level, which is consistent with the boiling phenomenon under the terrestrial gravity on Earth.

Figures 10–14 show the phase interface evolution during bubble detachment at different gravity levels when five magnetic fields of 5, 10, 15, 20, and 25 kA/m are applied, respectively. The phase interface evolution of the MNF film boiling without a magnetic field at different gravity levels is described. When the superheat is 2 K, the process of bubble growth and detachment is periodic. From Figures 10–14, it can be seen that whether the periodicity lasts depends on the magnetic field intensity applied. When it is 5, 10, or 15 kA/m, the magnetic field is relatively weak and has little influence on the flow field. At this time, the growth and bubble detachment remain periodic under the three gravity levels. It should be noted that, as seen in Figures 10a, 11a, and 12a,b, during the entire boiling process, the bubble growth and detachment among the bubble formation sites are not always synchronized; there is a certain delay. Furthermore, due to the horizontal magnetic force caused by the non-uniform magnetic field, the position of the bubble formation sites will undergo a certain lateral displacement. However, the bubbles at each bubble formation site always grow and detach periodically and continuously. Therefore, for this situation, we can assume that the growth and detachment of the bubbles are still periodic. As the magnetic field intensity increases to 20 kA/m, the bubble growth and detachment remain periodic under terrestrial gravity. However, when the gravity level is reduced to g/g_e = 0.44 or 0.11, the influence of the magnetic field on the phase interface evolution becomes more significant, and then the periodicity disappears. With the magnetic field force, the phase interface perturbation increases, and the numbers of bubble formation sites increase. Because of the horizontal component of the magnetic field force, the bubble formation sites will also merge, and when the stable state is reached, two or three bubble formation sites appear alternately. In addition, when the intensity is 20 kA/m, vapor columns begin to appear under reduced gravity. When it is further increased to 25 kA/m, the bubble growth and detachment process under terrestrial gravity on Earth becomes more disordered and loses its periodicity. The flow state completely enters the vapor column flow at the three gravity levels. From Figures 10–14, it is also obvious that when the intensity is 5, 10, or 15 kA/m, the growth and detachment processes of the bubbles at the three gravity levels are greatly different; however, the differences become smaller and smaller when the intensity reaches 20 or 25 kA/m. Especially for the case where the intensity reaches 25 kA/m, the bubble growth and detachment processes at the three gravity levels are already very similar. Therefore, the phase interface evolution during the bubble growth and detachment also illustrates that the application of a magnetic field can control the boiling phenomenon and eliminate the limitation of the gravity level.

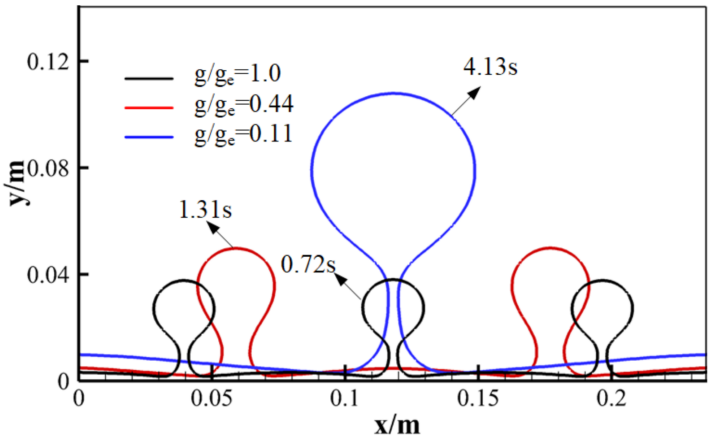

(**a**)

Figure 8. *Cont.*

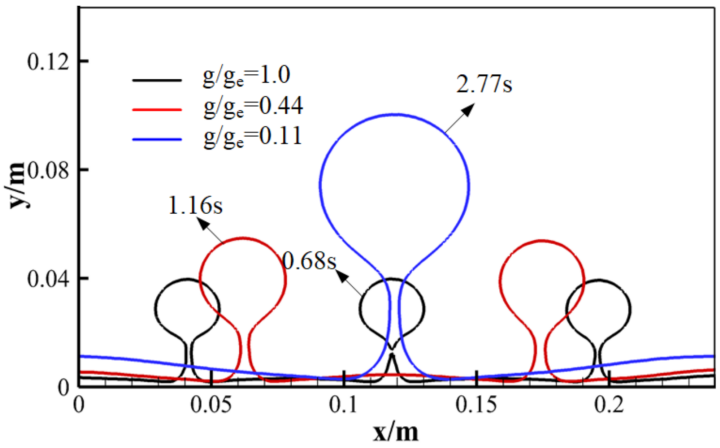

(**b**)

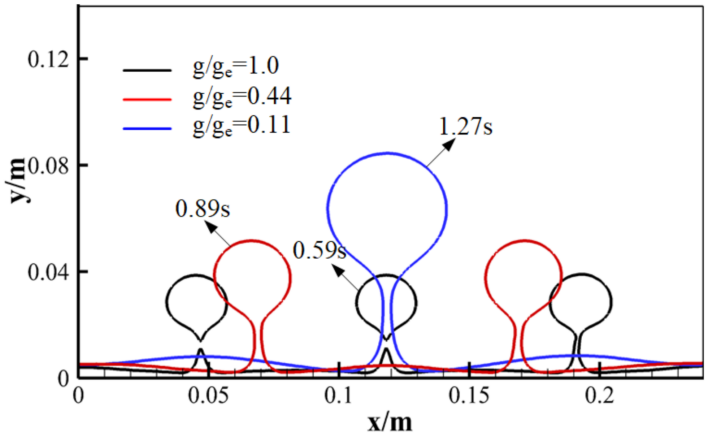

(**c**)

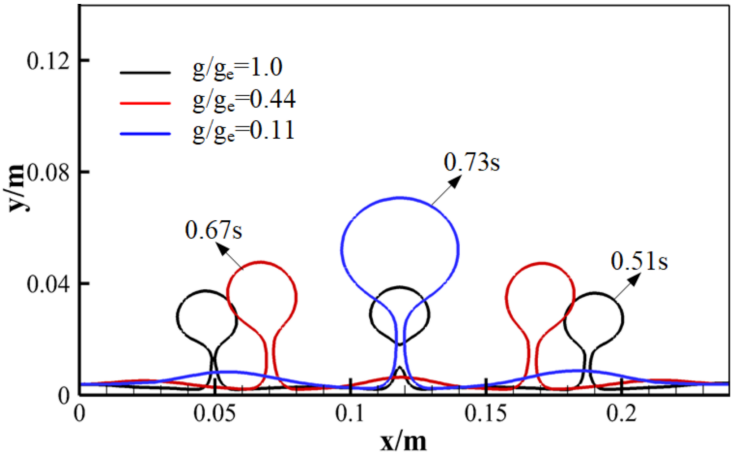

(**d**)

Figure 8. *Cont*.

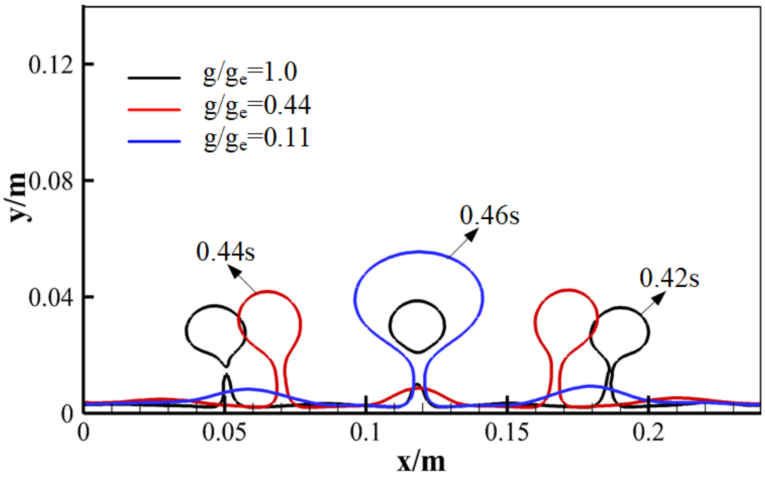

(**e**)

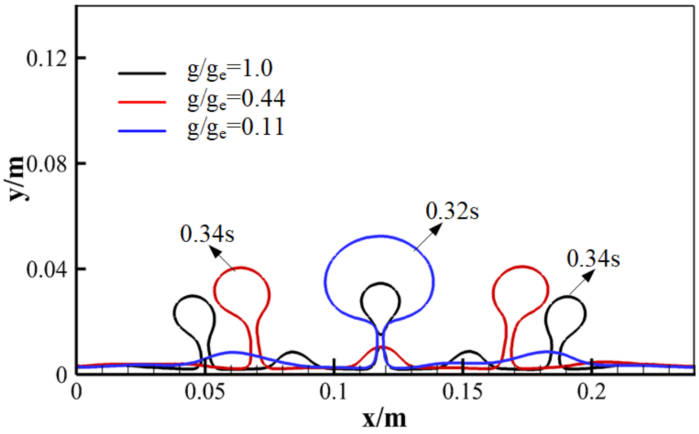

(**f**)

Figure 8. Effect of the magnetic field intensity on the departure of the first set of bubbles at different gravity levels. (**a**) H_0 = 0 kA/m, (**b**) H_0 = 5 kA/m, (**c**) H_0 = 10 kA/m, (**d**) H_0 = 15 kA/m, (**e**) H_0 = 20 kA/m, and (**f**) H_0 = 25 kA/m.

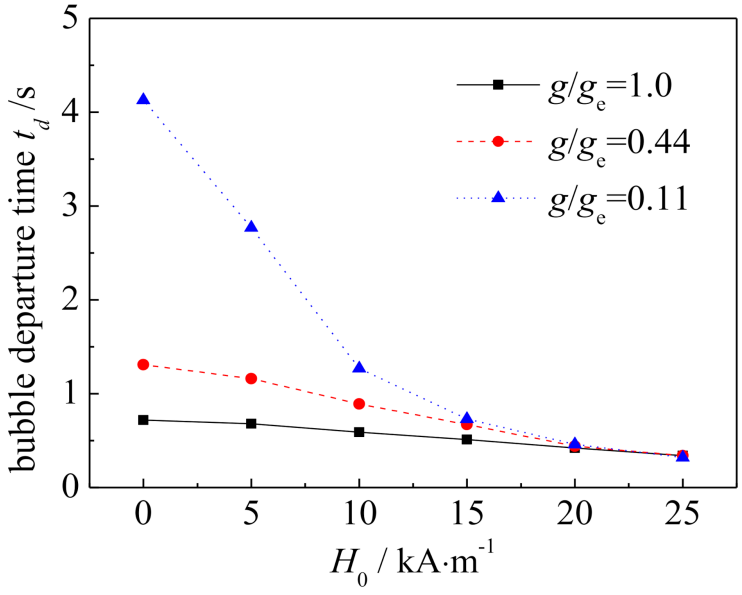

Figure 9. Variation of the bubble departure time with the magnetic field intensity at different gravity levels.

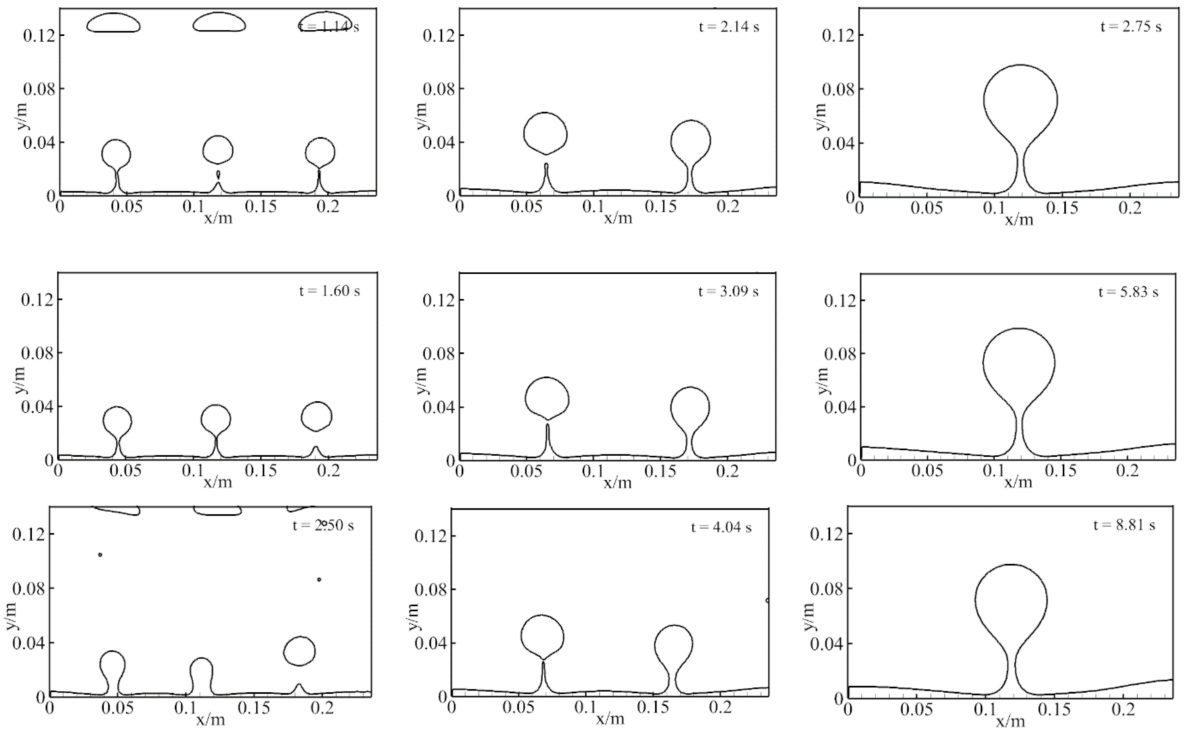

Figure 10. The bubble detachment at different gravity levels when H_0 = 5 kA/m. (**a**) g/g_e = 1.0, (**b**) g/g_e = 0.44, and (**c**) g/g_e = 0.11.

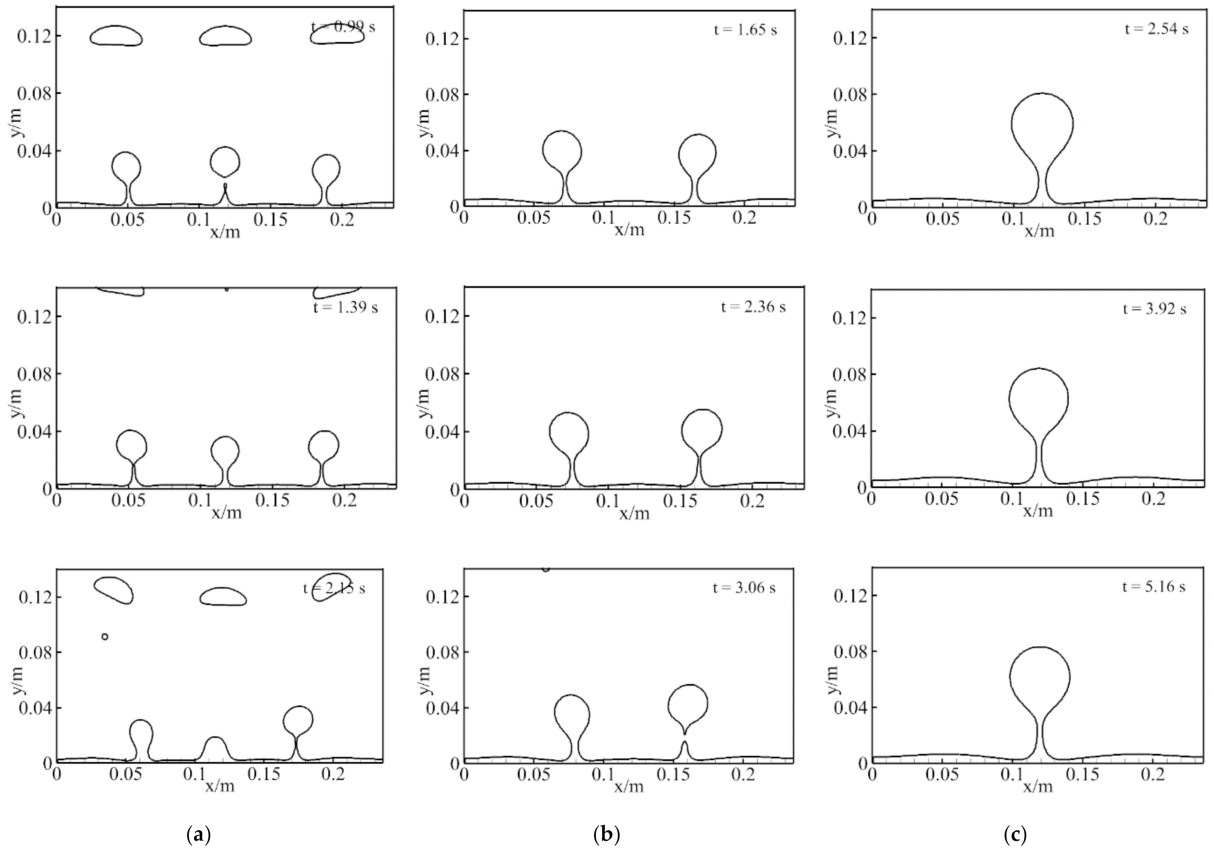

Figure 11. The bubble detachment at different gravity levels when H_0 = 10 kA/m. (**a**) g/g_e = 1.0, (**b**) g/g_e = 0.44, and (**c**) g/g_e = 0.11.

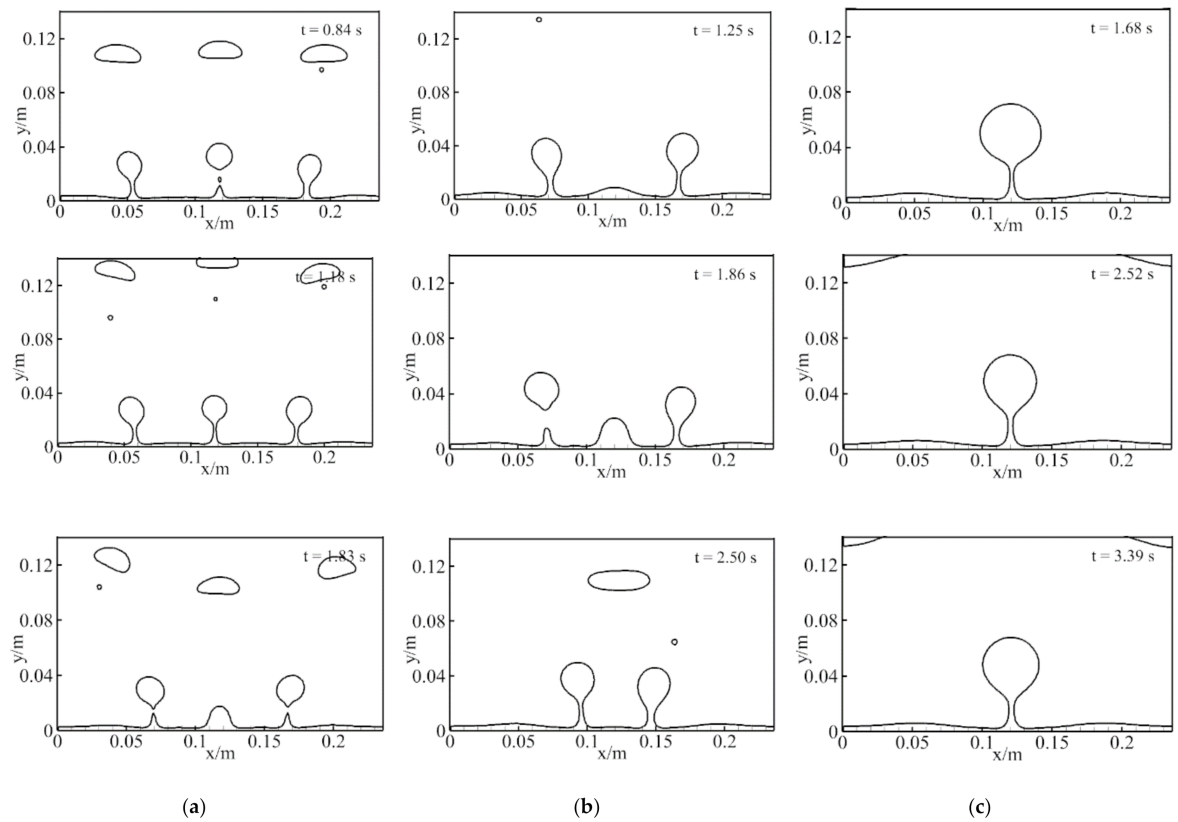

Figure 12. The bubble detachment at different gravity levels when H_0 = 15 kA/m. (**a**) g/g_e = 1.0, (**b**) g/g_e = 0.44, and (**c**) g/g_e = 0.11.

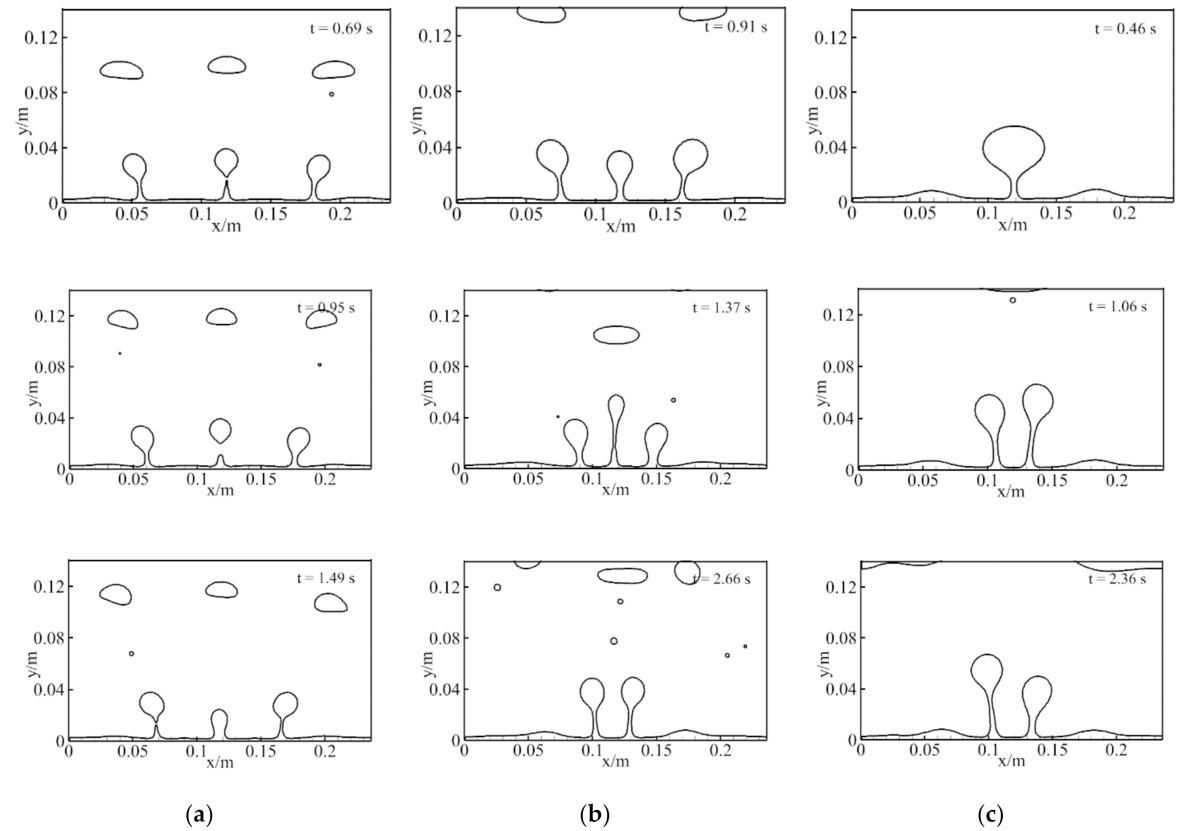

Figure 13. The bubble detachment at different gravity levels when H_0 = 20 kA/m. (**a**) g/g_e = 1.0, (**b**) g/g_e = 0.44, and (**c**) g/g_e = 0.11.

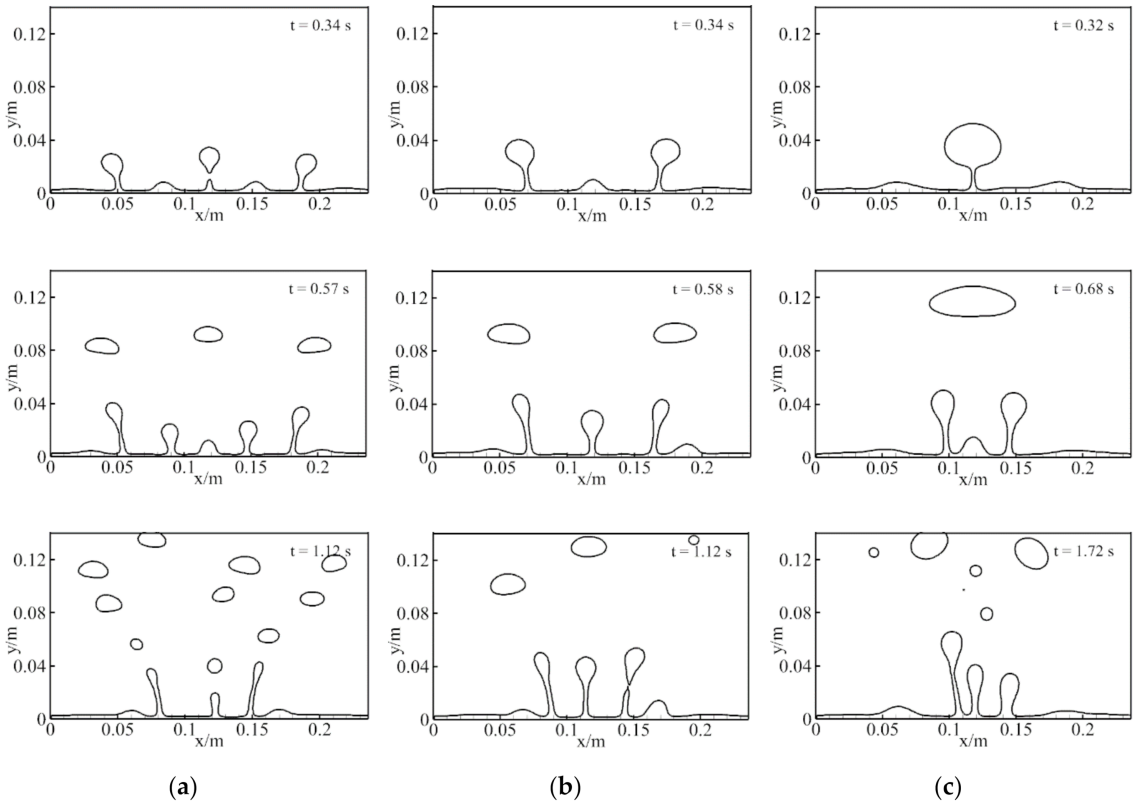

Figure 14. The bubble detachment at different gravity levels when H_0 = 25 kA/m. (**a**) g/ge = 1.0, (**b**) g/ge = 0.44, and (**c**) g/ge = 0.11.

3.2.2. Heat Transfer Characteristics

Figure 15 displays the variation curve of the space-averaged heat flux over time at different gravity levels when no magnetic field is applied and the five magnetic fields of H_0 = 5, 10, 15, 20, and 25 kA/m are applied. In Figures 6 and 15, it is shown that the heat transfer characteristics of the film boiling under a non-uniform magnetic field are slightly different from those under a uniform magnetic field. When the intensity is 5 or 10 kA/m, the space-averaged heat flux over time at the three gravity levels always remains periodic, as shown in Figure 15b,c. When the intensity reaches 15 kA/m, the change of the space-averaged heat flux over time at the two gravity levels of g/g_e = 1.0 and = 0.11 still remains periodic; however, the periodicity disappears at g/g_e = 0.44, which is shown in Figure 15d. When the intensity further reaches 20 kA/m, only the change of the space-averaged heat flux over time under terrestrial gravity on Earth remains periodic, while the periodicity disappears at the other two low gravity levels, as shown in Figure 15e. When the intensity reaches 25 kA/m, as shown in Figure 15f, the change of the space-averaged heat flux at the three gravity levels is very different from the other magnetic field intensities mentioned above. After reaching the stable stage, the three curves fluctuate a little, and the space-averaged heat flux changes a little. Moreover, the space-averaged heat flux at the three gravity levels is very close, which could be explained by the evolution of the bubble phase interface in Figure 14. When the intensity increases to 25 kA/m, the phase interface evolution during the bubble growth and detachment at the three gravity levels is very similar, and the flow states all enter into a stable vapor column flow.

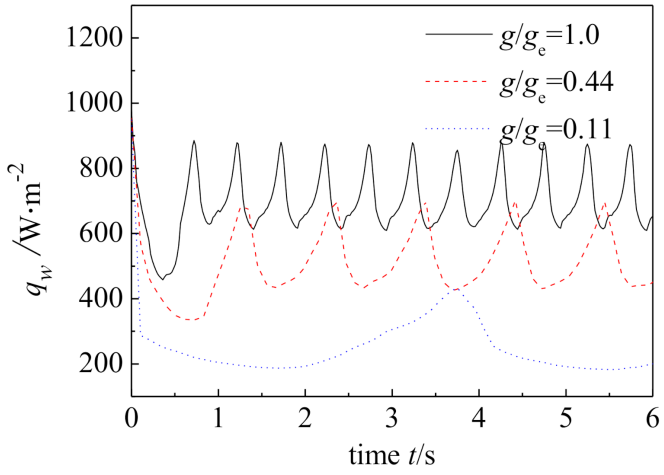

(**a**)

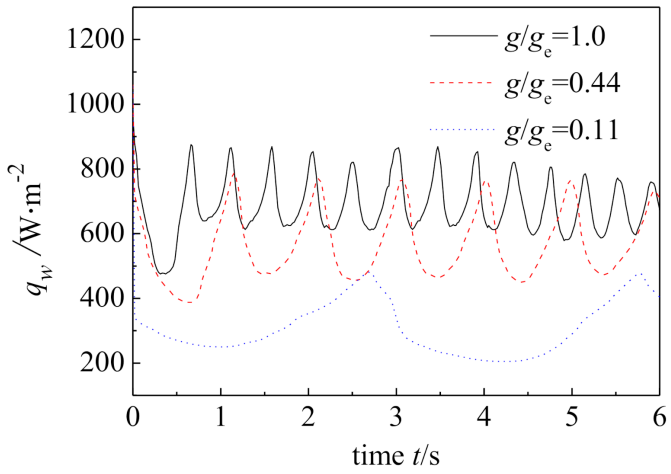

(**b**)

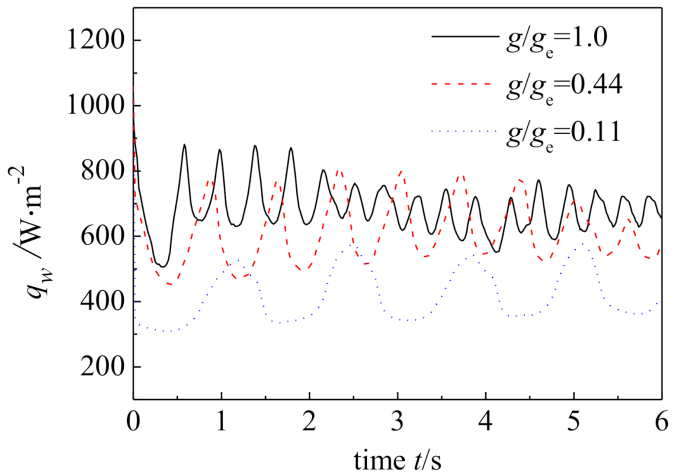

(**c**)

Figure 15. *Cont.*

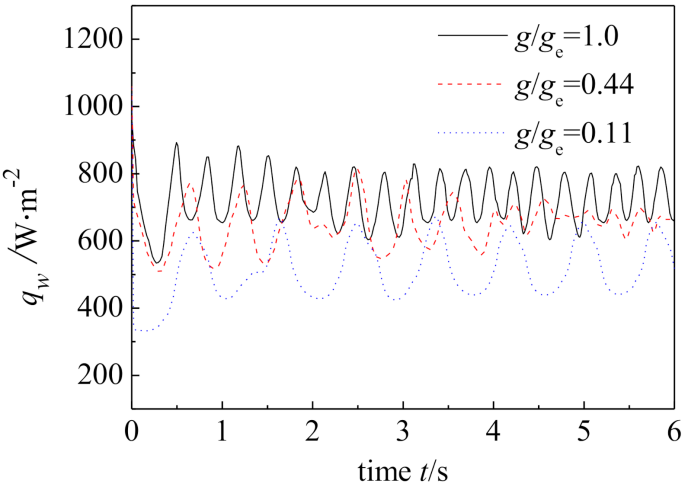

(**d**)

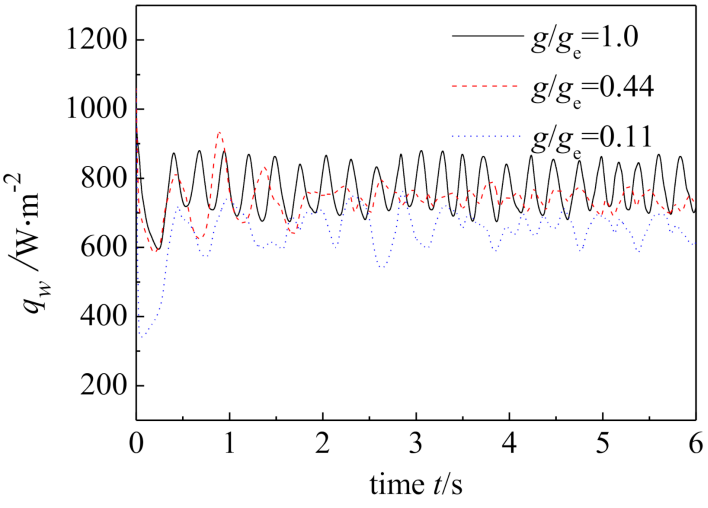

(**e**)

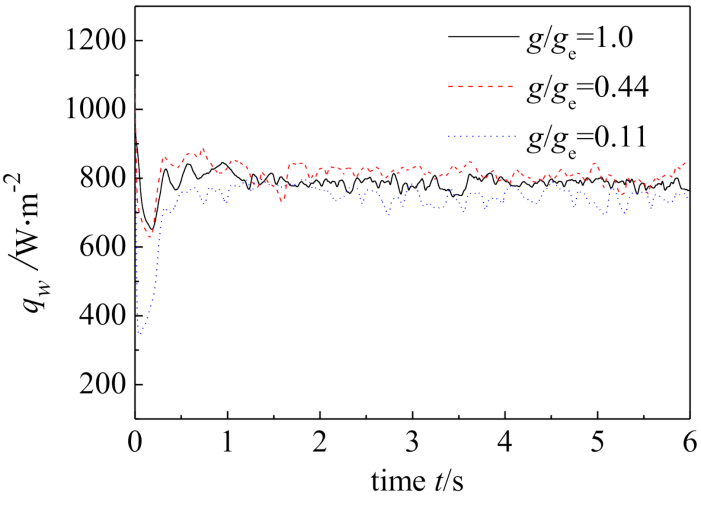

(**f**)

Figure 15. Influence of the magnetic field intensity on the variation of the space-averaged heat flux in different gravity conditions. (**a**) H0 = 0 kA/m, (**b**) H0 = 5 kA/m(**c**) H0 = 10 kA/m, (**d**) H0 = 15 kA/m, (**e**) H0 = 20 kA/m, and (**f**) H0 = 25 kA/m.

Referring to the distribution of the space- and time-averaged heat flux and the enhancement ratios at different gravity levels when applying a uniform magnetic field, for the non-uniform magnetic field, Figure 16 also shows the variation of the averaged heat flux and the ratio e with the intensity at different gravity levels. It is shown in Figures 7 and 16 that the heat transfer laws of the uniform and non-uniform magnetic fields are basically consistent. In a non-uniform magnetic field, when the intensity reaches 25 kA/m, the averaged heat flux under the three gravity levels is almost equal. Table 3 also gives the averaged heat flux and heat flux enhancement ratio under a non-uniform magnetic field. Therefore, it can be concluded that when the intensity increases to 25 kA/m, the boiling heat transfer characteristics under reduced gravity are basically the same as those on Earth.

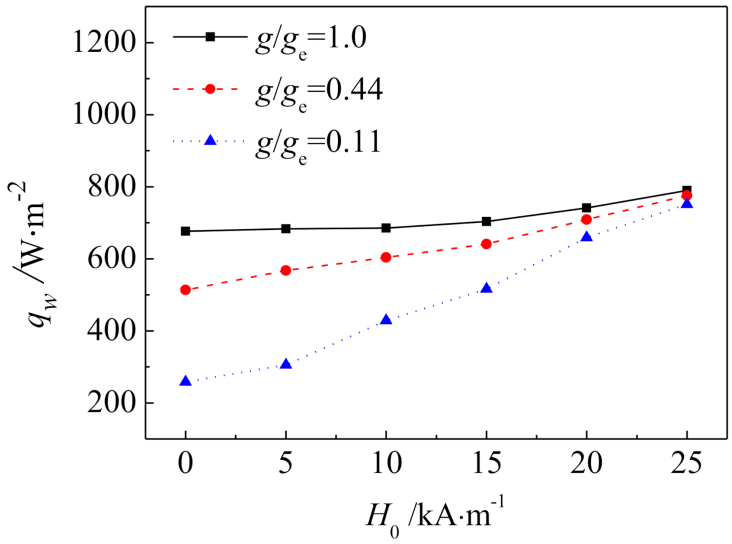

(**a**)

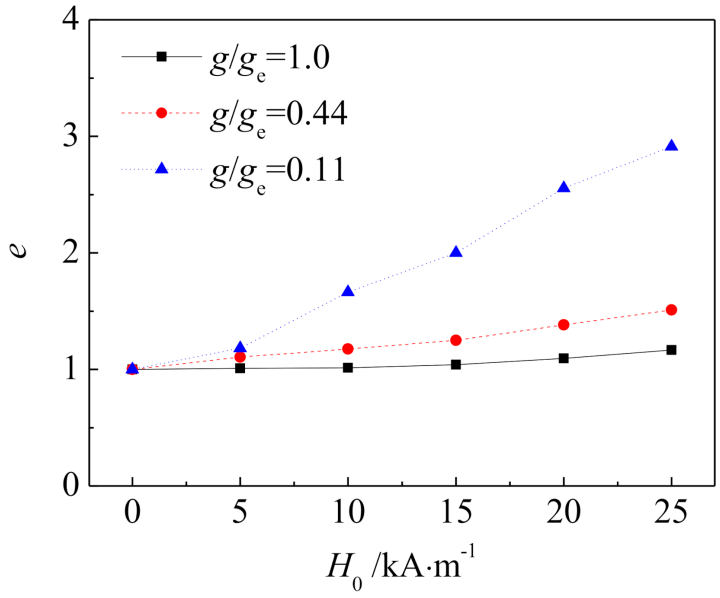

(**b**)

Figure 16. Variations of the (**a**) averaged heat flux and the (**b**) heat flux enhancement ratio under the non-uniform magnetic field (see Figure 3).

Table 3. Averaged heat flux and heat flux enhancement ratio under a non-uniform magnetic field.

g/g_e	q_0 (W/m^2)	5 kA/m		10 kA/m		15 kA/m		20 kA/m		25 kA/m	
		q_m (W/m^2)	e	q_m (W/m^2)	e	q_m (W/m^2)	e	q_m (W/m^2)	e	q_m (W/m^2)	e
1.0	677	683	1.01	685	1.01	704	1.04	741	1.09	789	1.17
0.44	513	567	1.1	603	1.18	641	1.25	709	1.38	776	1.51
0.11	258	305	1.18	429	1.66	516	2.00	659	2.55	751	2.91

4. Conclusions

Compared with the results on Earth, an MNF's boiling heat transfer under reduced gravity is more complex. Reducing or even eliminating the effect of gravity on the boiling heat transfer process, restraining the appearance of abnormally large bubbles, and preventing significant decreases in Critical Heat Flux (CHF) will be the key to enhancing boiling heat transfer in low gravity levels. In this study, a computational model of MNF boiling flow was developed and adopted to investigate the heat transfer characteristics and thermodynamic characteristics of the phase interface during boiling of MNF-saturated film under low gravity. The following conclusions were obtained by studying the three situations of a non-magnetic field, a uniform magnetic field, and a non-uniform magnetic field in detail.

The thermodynamic characteristics of the phase interface in the MNF film boiling process under different gravity levels and uniform and non-uniform magnetic fields were studied. After the magnetic field is applied, as the magnetic field intensity increases, the differences among the evolution modes of the phase interface under different gravity levels become smaller and smaller. The bubble flow during boiling of the film without the magnetic field turns into a column flow when the intensity increases to 25 kA/m, and phase interface evolution mode is basically the same at different gravity levels. The results indicate that applying a magnetic field can effectively solve the problem of abnormally large bubbles in the boiling process under low gravity, and can make the phase interface evolution under low gravity close to the evolution process under the Earth's gravity.

After the magnetic field is applied, with the increase of the magnetic field's intensity, the differences among the heat transfer characteristics of the film boiling under the three gravity levels become smaller and smaller; the lower the gravity level, the greater the effect of the magnetic field on heat transfer. The results show that by applying a magnetic field of a certain intensity, the boiling heat transfer characteristics under low gravity levels are basically the same as those under Earth's gravity, and the problem of significantly reduced heat flux under low gravity levels can be solved.

Author Contributions: Conceptualization, K.G. and H.L.; methodology, K.G.; software, K.G.; validation, K.G. and F.C.; investigation, K.G.; writing—original draft preparation, K.G.; writing—review and editing, F.C.; All authors have read and agreed to the published version of the manuscript.

Funding: This research was funded by the joint fund between the Chinese Academy of Sciences (CAS) and the National Natural Science Foundation of China (NSFC), grant number U1738105.

Institutional Review Board Statement: Not applicable.

Informed Consent Statement: Not applicable.

Conflicts of Interest: The authors declare no conflict of interest.

Abbreviations

B	magnetic induction intensity (T)
c	volume fraction of the discrete phase
c_p	specific heat (J/kg·K)
d	distance (m)
e	heat flux enhancement ratio

$\mathbf{F}_\sigma$	surface tension (N/m^2)
$\mathbf{F}_m$	magnetic force (N/m^2)
$\mathbf{g}$	gravitational acceleration (m/s^2)
$\mathbf{H}$	magnetic field intensity (A/m)
$H(\phi)$	smooth Heaviside function
h	grid size (m)
h_{lg}	latent heat of vaporization (J/kg)
$\mathbf{M}$	magnetization (A/m)
$\dot{m}$	mass transfer rate (kg/m^3.s)
p	pressure (pa)
$\dot{q}$	heat flux that causes the phase change at the phase interface (W/m^2)
s	width of transition region for smoothing (m)
T	temperature (°C)
$\mathbf{u}$	velocity (m/s)
Greek letters	
β_T	volume expansion coefficient
$\delta(\phi)$	Dirac delta function
η	dynamic viscosity (kg/m·s)
κ	phase interface curvature (1/m)
λ	thermal conductivity (W/m·K)
μ	magnetic permeability (H/m)
μ_0	vacuum permeability $\mu_0 = 4\pi \times 10^{-7}$ H/m
ρ	density (kg/m^3)
σ	surface tension coefficient (N/m)
Γ	phase interface
ϕ	level-set function
φ	volume concentration of nanoparticles
χ	magnetic susceptibility
ψ	magnetic potential (At)
Ω	control volume unit
Subscripts	
e	Earth
g	discrete phase
l	continuous phase
mix	mixture phase
p	magnetic nanoparticles
w	wall
Acronym	
MNF	magnetic nanofluid

References

1. Xue, Y.F.; Zhao, J.F.; Wei, J.J.; Li, J.; Guo, D.; Wan, S.X. Experimental study of nucleate pool boiling of FC-72 on smooth surface under microgravity. *Microgravity Sci. Technol.* **2011**, *23*, S75–S85. [CrossRef]
2. Oka, T.; Abe, Y.; Mori, Y.H.; Nagashima, A. Pool boiling heat transfer in microgravity (experiments with CFC-113 and water utilizing a drop shaft facility). *Int. J. Ser. B Fluids Therm. Eng.* **1996**, *39*, 798–807. [CrossRef]
3. Sodtke, C.; Kern, R.; Schweizer, N.; Stephan, P. High resolution measurements of wall temperature distribution underneath a single vapour bubble under low gravity conditions. *Int. J. Heat Mass Transf.* **2006**, *49*, 1100–1106. [CrossRef]
4. Souza, R.R.; Passos, J.C.; Cardoso, E.M. Confined and unconfined nucleate boiling under terrestrial and microgravity conditions. *Appl. Therm. Eng.* **2013**, *51*, 1290–1296. [CrossRef]
5. Lee, H.S.; Merte, H. Hemispherical vapor bubble growth in microgravity: Experiments and model. *Int. J. Heat Mass Transf.* **1996**, *39*, 2449–2461. [CrossRef]
6. Dhir, V.K.; Warrier, G.R.; Aktinol, E.; Chao, D.; Eggers, J.; Sheredy, W.; Booth, W. Nucleate pool boiling experiments (NPBX) on the international space station. *Microgravity Sci. Technol.* **2012**, *24*, 307–325. [CrossRef]
7. Konishi, C.; Mudawar, I. Review of flow boiling and critical heat flux in microgravity. *Int. J. Heat Mass Transf.* **2015**, *80*, 469–493. [CrossRef]
8. Zhao, J.F.; Li, Z.D.; Zhang, L.; Li, J.C.; Fu, S. Numerical simulation of single bubble pool boiling in different gravity conditions. *AIP Conf. Proc.* **2011**, *1376*, 565–568.

9. Ma, X.J.; Cheng, P.; Gong, S.; Quan, X.J. Mesoscale simulations of saturated pool boiling heat transfer under microgravity conditions. *Int. J. Heat Mass Transf.* **2017**, *114*, 453–457. [CrossRef]
10. Pandey, V.; Biswas, G.; Dalal, A. Saturated film boiling at various gravity levels under the influence of electrohydrodynamic forces. *Phys. Fluids* **2017**, *29*, 032104. [CrossRef]
11. Liu, J.H.; Gu, J.M.; Lian, Z.W.; Liu, H. Experiments and mechanism analysis of pool boiling heat transfer enhancement with water-based magnetic fluid. *Heat Mass Transf.* **2004**, *41*, 170–175.
12. Lee, J.H.; Lee, T.; Jeong, Y.H. Experimental study on the pool boiling CHF enhancement using magnetite-water nanofluids. *Int. J. Heat Mass Transf.* **2012**, *55*, 2656–2663. [CrossRef]
13. Abdollahi, A.; Salimpour, M.R. Experimental investigation on the boiling heat transfer of nanofluids on a flat plate in the presence of a magnetic field. *Eur. Phys. J. Plus* **2016**, 131. [CrossRef]
14. Abdollahi, A.; Salimpour, M.R.; Etesami, N. Experimental analysis of magnetic field effect on the pool boiling heat transfer of a ferrofluid. *Appl. Therm. Eng.* **2017**, *111*, 1101–1110. [CrossRef]
15. Amirzehni, R.; Aminfar, H.; Mohammadpourfard, M. Experimental study of magnetic field effect on bubble lift-off diameter in sub-cooled flow boiling. *Exp. Therm. Fluid Sci.* **2017**, *89*, 62–71. [CrossRef]
16. Guo, K.K.; Li, H.X.; Feng, Y.; Wang, T.; Zhao, J.F. Numerical simulation of magnetic nanofluid (MNF) film boiling using the VOSET method in presence of a uniform magnetic field. *Int. J. Heat Mass Transf.* **2019**, *134*, 17–29. [CrossRef]
17. Guo, K.K.; Li, H.X.; Feng, Y.; Wang, T.; Zhao, J.F. Enhancement of non-uniform magnetic field on saturated film boiling of magnetic nanofluid (MNF). *Int. J. Heat Mass Transf.* **2019**, *143*, 12. [CrossRef]
18. Ki, H. Level set method for two-phase incompressible flows under magnetic fields. *Comput. Phys. Commun.* **2010**, *181*, 999–1007. [CrossRef]
19. Ansari, M.R.; Hadidi, A.; Nimvari, M.E. Effect of a uniform magnetic field on dielectric two-phase bubbly flows using the level set method. *J. Magn. Magn. Mater.* **2012**, *324*, 4094–4101. [CrossRef]
20. Shi, D.X.; Bi, Q.C.; Zhou, R.Q. Numerical simulation of a falling ferrofluid droplet in a uniform magnetic field by the VOSET method. *Numer. Heat Transf. Part A Appl.* **2014**, *66*, 144–164. [CrossRef]
21. Sun, D.L.; Tao, W.Q. A coupled volume-of-fluid and level set (VOSET) method for computing incompressible two-phase flows. *Int. J. Heat Mass Transf.* **2010**, *53*, 645–655. [CrossRef]
22. Wang, T.; Li, H.X.; Zhang, Y.F.; Han, W.; Sheng, T.Y.; Zhang, W.Q. Numerical simulation of two-phase flows using 3D-VOSET method on dynamically adaptive octree grids. In Proceedings of the 22nd International Conference on Nuclear Engineering, Prague, Czech Republic, 7–11 July 2014.
23. Brackbill, J.U.; Kothe, D.B.; Zemach, C. A continuum method for modeling surface tension. *J. Comput. Phys.* **1992**, *100*, 335–354. [CrossRef]
24. Ling, K.; Son, G.; Sun, D.L.; Tao, W.Q. Three dimensional numerical simulation on bubble growth and merger in microchannel boiling flow. *Int. J. Therm. Sci.* **2015**, *98*, 135–147. [CrossRef]
25. Udaykumar, H.S.; Mittal, R.; Shyy, W. Computation of solid–liquid phase fronts in the sharp interface limit on fixed grids. *J. Comput. Phys.* **1999**, *153*, 535–574. [CrossRef]
26. Rosensweig, R.E. *Ferrohydrodynamics*; Cambridge University Press: Cambridge, UK, 1985.